Published by IOP Publishing for Sissa Medialab

Received: *September 28, 2025*
Revised: *November 28, 2025*
Accepted: *December 4, 2025*
Published: *January 9, 2026*

26th International Workshop on Radiation Imaging Detectors
Bratislava, Slovakia
6–10 July 2025

Preparing Timepix3 for deployment in low-radioactivity natural settings: an integrated workflow for charged particle detection and imaging

R. Kumar[a,b,*] **D. Wood**,[c] **M. Frouin**,[e] **R. Plackett**,[c] **C. Osborne**,[a] **M.A. Hill**[d] **and J-L. Schwenninger**[a]

[a] *Radiation Physics Research Group, UGCT, Department of Physics and Astronomy, Ghent University, Proeftuin Campus, 9000, Gent, Belgium*
[b] *Oxford Luminescence Dating Laboratory, RLAHA, School of Archaeology, University of Oxford, Oxford, OX1 3TG, U.K.*
[c] *Department of Physics, University of Oxford, Parks Road, Oxford, OX1 3PU, U.K.*
[d] *Department of Oncology, University of Oxford, Old Road Campus Research Building, Roosevelt Drive, Oxford, OX3 7DQ, U.K.*
[e] *Department of Geosciences, University of Stony Brook, Stony Brook, NY 11794-21, U.S.A.*

E-mail: raju.kumar@ugent.be

Abstract: The natural sedimentary environment possesses a mixed field of α-, β-, and γ-radiation emitted from the radioactive decay of radionuclides such as potassium-40 (K-40), uranium-238 (U-238), and thorium-232 (Th-232). These emissions are responsible for dose accumulation in feldspar and quartz mineral grains, forming the basis of luminescence dating. The inhomogeneous spatial distribution of radionuclides in sediments and local energy deposition at the grain level can cause microdosimetric variations, contributing to overdispersion in equivalent dose (D_e) distributions. Understanding and resolving these variations requires a detector that can simultaneously map various types of radiation and their energy deposition at the micron scale.

Here we present a workflow for configuring and applying Timepix3 (silicon-based hybrid pixel detector, $14 \times 14\,\mathrm{mm}^2$ active area, 256×256 pixels, 300 µm thickness) for high-sensitivity imaging of α- and β-particles simultaneously in mixed-radiation fields. The workflow includes particle-track reconstruction, charged-particle identification, background suppression, and energy calibration with a

*Corresponding author.

https://doi.org/10.1088/1748-0221/21/01/C01010

mixed α-particle source (Pu-239, Am-241, Cm-244; 5.15–5.80 MeV) in air. A linear energy calibration response was obtained; however, the detector was unable to fully resolve three α-particle peaks. While this appears to be a limitation, it ultimately provides insights into the detector's response under conditions that closely mimic the energy spectra of natural radiation, broad energy distributions, and measurement conditions such as ambient atmospheric pressure.

KEYWORDS: Microdosimetry and nanodosimetry; Pattern recognition, cluster finding, calibration and fitting methods

2026 JINST 21 C01010

Contents

1 Introduction

Luminescence dating is a radiometric tool for determining the age of geo-archaeological events by measuring the radiation dose accumulated in the lattices of quartz and feldspar minerals, since their last exposure to light or heat [1, 2]. The accuracy and precision of this method depend heavily on understanding how natural radiation, primarily from K-40, U-238, and Th-232, deposits energy at the grain level [3]. Variations in energy deposition at the grain level (microdosimetry) can cause overdispersion in equivalent or total absorbed dose (D_e) distributions from individual mineral grains of the same sample and limit chronological precision [4, 5]. Tackling microdosimetry warrants studying the spatial distribution of K-40, U-238, and Th-232 radionuclides around quartz and feldspar mineral grains, as well as their respective contributions to local energy deposition and dose rate. Supplementary figure S1 illustrates how energy deposition varies among individual mineral grains (90–300 µm) in a natural setting due to emanating α-, β-, and γ-radiation.

Conventional techniques, such as Micro X-Ray Fluorescence (µXRF) or Inductively Coupled Plasma Mass Spectrometry (ICP-MS, including laser ablation setups), can provide elemental maps or isotope-specific concentrations, but they cannot track individual particle interactions or map grain-level energy deposition. The extremely low activity levels in natural sedimentary environments further limit their usefulness, demanding highly sensitive detectors that can operate efficiently in low-flux conditions. Additionally, the natural radiation fields comprise a complex mixture of α-, β-, and γ-radiation, which necessitates the use of complementary detectors to capture and analyze all components [6].

Timepix, a hybrid pixel detector, [7] addresses these limitations by offering high-resolution, energy-resolved, particle-specific grain-scale measurements while operating effectively in low-flux environments due to its high sensitivity [8]. Its ability to detect and map individual charged particles (α and β) eliminates assumptions about isotopic uniformity, particle range, and local geometry that are inherent in bulk or indirect methods. Moreover, by capturing both the energy deposition and spatial track of particles, Timepix can reveal localized α/β-emitting 'hotspots', providing a degree of microdosimetric insight not possible with conventional methods. These capabilities make Timepix a promising tool for studying radionuclide distributions and microdosimetry in natural environments or samples.

Although the present study does not yet include measurements in natural settings, it is intended to lay the groundwork for future research. To apply Timepix to a low-radioactivity sedimentary environ-

2026 JINST 21 C01010

ment, it is essential first to characterize the detector's response under controlled, higher-flux laboratory conditions and to develop robust data-analysis methods capable of identifying and separating sparse α, β, and γ events from mixed radiation fields. Therefore, we focus here on developing an in-house but effective particle-tracking and reconstruction algorithm capable of separating α, β, and γ events from mixed radiation frames, tailored for low-flux imaging. We then demonstrate the use of a mixed α-particle calibration source (Pu-239, Am-24, and Cm-244) to calibrate Timepix3 (a Timepix-family detector) at high energies in air. Using a mixed source rather than a single emitter better reproduces the diversity of particle energies expected in natural environments, even though the flux is higher.

This preparation, including detector characterization, calibration, and algorithm development, is therefore a necessary step toward the ultimate goal of deploying Timepix3 in low-radioactivity natural settings to map energy-resolved α- and β-particle emissions, determine radionuclide distributions at the grain scale, and investigate grain-scale energy-deposition behavior, i.e., microdosimetry.

2 Timepix3 and calibration source

For this study, a Timepix3 hybrid pixel detector (silicon sensor material, 300 µm thickness, 256× 256 pixels, 55 µm pitch), equipped with an ADVACAM reader, was employed (figure 1a). Timepix3 primarily operates in two modes: frame mode and event-driven mode. In event-driven mode, each pixel independently records the Time-over-Threshold (ToT), which is proportional to the deposited energy, and the Time-of-Arrival (ToA), which records the precise arrival time of each particle, enabling simultaneous measurement of energy and time at the single-particle level (figure 1b and c; [8, 9]). By leveraging this information, individual particles can be tracked based on their footprints across the pixel array and identified as α, β, γ, or other particles, including photons and cosmic rays. Figure S2 illustrates examples of different particle types and their characteristic tracks on the Timepix3 sensor: dots and small blobs correspond to low-energy photons or electrons, curly tracks indicate high-energy photons or electrons, heavy blobs correspond to α particles, and straight tracks are characteristic of cosmic rays [10].

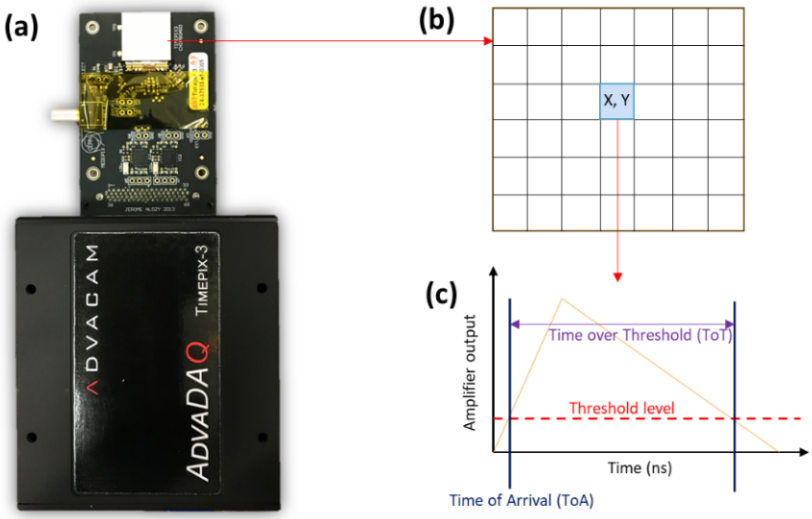

Figure 1. (a) Image of Timepix3 with an ADVACAM reader. (b) Schematic of the pixel matrix (256 × 256 pixels, 55 µm pitch). Indicated X and Y represent the pixel's row and column. (c) Representation of how Timepix3 detects a particle and assigns ToA and ToT values to a specific matrix index.

2026 JINST 21 C01010

A Pixet Pro (v1.4) software was used for the operation and parametrization of Timepix3. The data were saved in a .t3pa file extension. Necessary preparation, including threshold equalization and low-energy calibration of the detector, was performed at the Physics Department of the University of Oxford (refer to figure S3). For data analysis, MATLAB (R2021-R2024b) software was used.

To calibrate Timepix3 for high-energy charged-particle detection, a mixed α-particle source comprising Pu-239, Am-241, and Cm-244 was used, which is expected to produce three distinct peaks at 5.15 MeV, 5.49 MeV, and 5.80 MeV, with each of these peaks accompanied by a smaller secondary peak at 5.14 MeV, 5.43 MeV, and 5.76 MeV. The major peaks correspond to the most probable α-decay energies, 5.15, 5.49, and 5.80 MeV, with branching probabilities of ~73%, 85%, and 77%, respectively. Secondary peaks at 5.14, 5.43, and 5.76 MeV, with ~15%, 13%, and 23% probabilities, arise from less probable transitions. The total activity of this source was 3 kBq about thirty years ago. Selection of a mixed source was intentional, as natural sedimentary environments contain charged particles of varying energies, and the mixed source allows the detector response to be evaluated under conditions that closely mimic the broad energy spectrum of natural radiation.

All the measurements were performed in a radiation-controlled laboratory at Oxford Luminescence Dating Laboratory, RLAHA, School of Archaeology, University of Oxford, UK. This laboratory contains multiple ^{90}Sr/^{90}Y β-sources, inducing a huge β-radiation background. To minimize this and other environmental radiation backgrounds, all measurements were conducted within lead shielding as shown in figures 2a, b, and c.

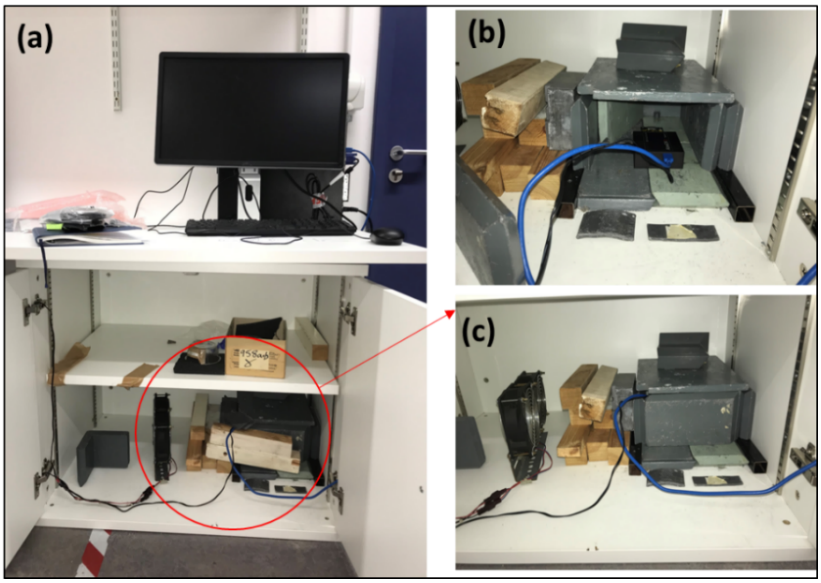

Figure 2. (a) The measurement setup. (b, c) Lead shielding for background suppression.

3 Particle reconstruction and identification

Based on the distinct tracks produced by different types of particles, an algorithm was developed in MATLAB to analyze and classify particle events. The first step in the algorithm is to label clusters of hits by grouping pixels with close ToA values. Once the clusters are labeled, the algorithm reconstructs the particle tracks for photons, electrons, and α-particles.

2026 JINST 21 C01010

For photons, the algorithm identifies clusters consisting of one to three adjacent pixel hits, as photon interactions typically produce small clusters. For α-particles, it makes use of their characteristic track shapes (heavy blobs) and energy deposition patterns. The algorithm first searches for the central hit pixel within each cluster and determines its matrix index (central index). It then examines the first layer of neighboring pixels through their indices (the eight nearest neighbors in vertical and horizontal directions) and determines what fraction of these neighbors are also part of the cluster. This ratio is defined as the first-layer fill factor, f_1, expressed as the percentage of neighboring pixels that belong to the cluster. The algorithm then extends the search to the second layer of neighbors surrounding the central hit. The fraction of these second-layer pixels that also belong to the cluster is defined as the second-layer fill factor, f_2.

By applying thresholds of $f_1 > 90\%$ and $f_2 > 40\%$, the algorithm was able to separate α-particle clusters with greater than 90% accuracy (figure 3a). An example of an α-particle cluster is demonstrated in figure 3b. The threshold level (THL) was set to 2.24 keV, so pixels with smaller deposited energies were excluded from cluster formation. All remaining clusters that did not meet the α-particle criteria and had a cluster size (total number of pixels in the cluster) greater than five were classified as electrons.

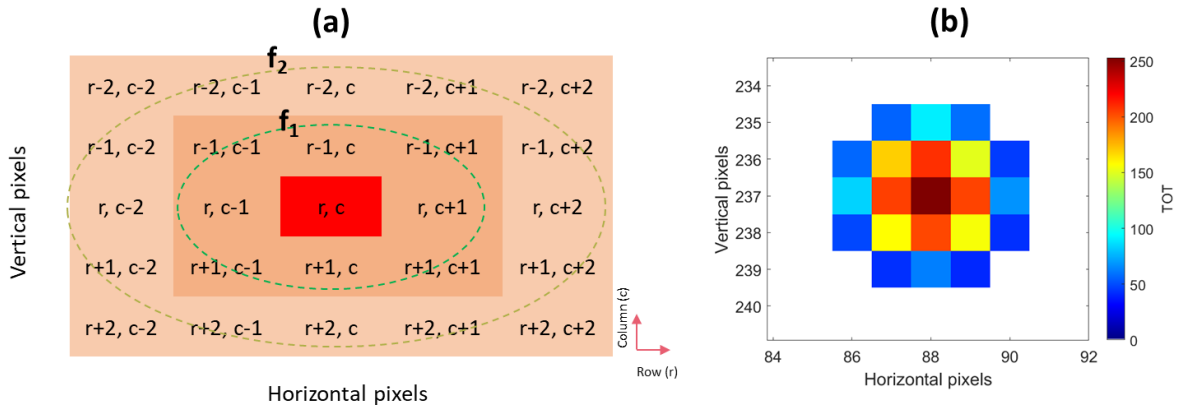

Figure 3. (a) Algorithm for identifying an α-cluster. (r, c) indicates the row and column of the central hit (pixel with the maximum ToT value), while (r ± 1, c ± 1) and (r ± 2, c ± 2) represent the neighboring pixels. f_1 and f_2 are fill factors representing the percentage of first- and second-layer neighboring pixels around the central-hit pixel that match the cluster, and they are compared to predefined thresholds to determine whether the cluster is classified as an α- or β-event. (b) Example of a homogeneous α-cluster showing its highest energy deposited in the central pixel.

Following the reconstruction and identification algorithm described above, photons, electrons, and α-particles can be effectively separated, as demonstrated in figure 4. Figure 4a shows a mixed distribution containing all particle types. When the algorithm is applied, the particles are successfully classified and separated, as depicted in figures 4b, c, and d, corresponding to photons, electrons, and α-particles, respectively.

After successfully separating particle types using the reconstruction algorithm, we evaluated background radiation, since the detector was operated in a radiation area. Figures S4a and S4b show the frames from six-hour measurements outside and inside the shielding. The detector was operated with a THL of 2.24 keV and 50 V bias. Shielding significantly reduced the background from 1482 to 193 cluster counts/hour: γ-photons background reduced from 1213 to 73 counts per hour, β-background reduced from 262 to 117 counts/hour, and α-particle background reduced from 7 to 3 counts/hour. These results confirm the effectiveness of the lead shielding in suppressing background radiation.

2026 JINST 21 C01010

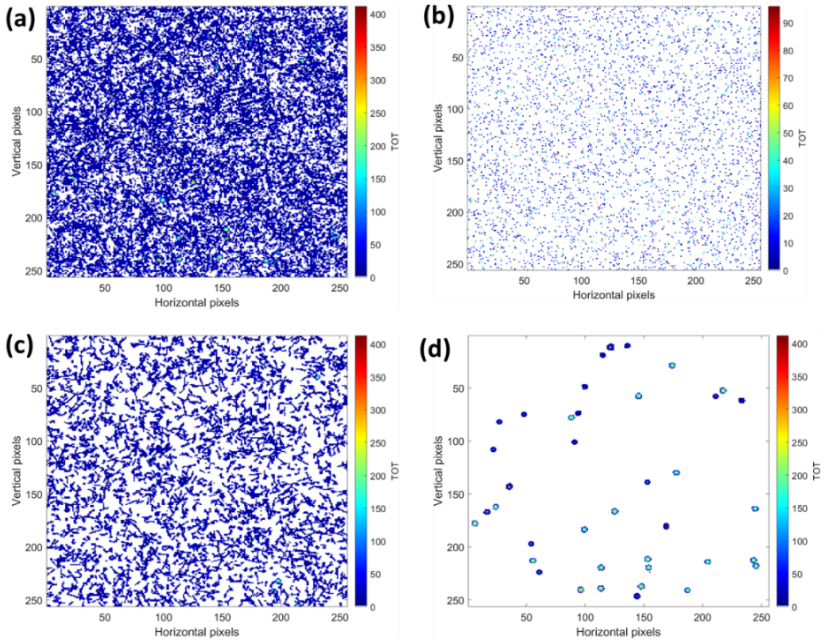

Figure 4. (a) A mixed radiation frame, acquired over 10 hours of period outside the lead shielding. Isolated (b) γ photons (c) β-particles or electrons and (c) α-particles using the algorithm discussed in section 3.

4 Detector calibration with α-calibration source

In this section, calibration with α-calibration source (Pu-239, Am-241, and Cm-244) was performed, and the effectiveness of Timepix3 in accurately measuring high-energy charged particles was evaluated.

4.1 Experimental setup

To calibrate the Timepix3 detector, we adopted a global calibration approach instead of pixel-wise calibration. The detector's distance from the α-source was varied to determine the optimal position where all α-particle peaks at 5.15 MeV, 5.49 MeV, and 5.80 MeV were maximally resolved (figure 5). Measurements were performed at six source-to-detector distances: 1.0 (closest), 1.3, 1.6, 1.9, 2.2,

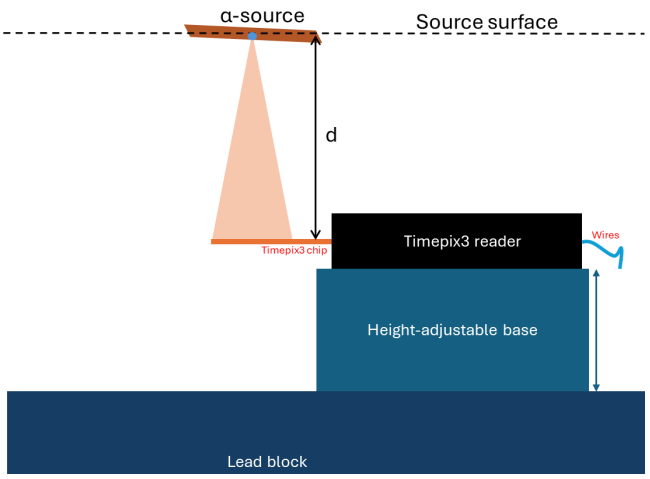

Figure 5. Experimental set up for the calibration of Timepix3.

2026 JINST 21 C01010

and 2.5 cm. Distances greater than 3.0 cm were excluded because the α-particles started to lose energy due to interaction with air molecules, which caused the clusters to become smaller. Operating the detector in a vacuum without active cooling led to overheating of the detector; therefore, all measurements were performed at ambient atmospheric pressure in lead shielding, which also reflects the measurement conditions found in the natural environment.

4.2 The α-particle spectra

Figure 6 shows the α-particle energy spectra (histogram) measured with the Timepix3 detector at three different source-to-detector distances: 1.0 cm (figure 6a), 2.2 cm (figure 6b), and 2.5 cm (figure 6c). Each spectrum was acquired over a 24-hour measurement period. The x-axis represents the ToT volume, defined as the summation of all Time-over-Threshold (ToT) counts within a single α-cluster, which corresponds to the total deposited energy in that cluster. To reduce background contributions, the α-clusters were reconstructed and classified using the algorithm described in section 3, rather than directly utilizing all the clusters. For these measurements, the fill factor thresholds were set to $f_1 > 90\%$ and $f_2 > 40\%$, ensuring identification of all the α-particle events. The THL was set at 2.24 keV, and a bias voltage of 50 V was applied to the detector for these measurements.

As is evident, the closest distance (1.0 cm) did not yield an optimal spectrum (figure 6a). Although the three main peaks are visible, they either sit on a significant continuous background or overlap with one another, including the smaller secondary peaks. The best energy resolution was achieved at a source-to-detector distance of ~2.2 cm (figure 6b), where the peaks are well defined. At a little further distance (2.5 cm; figure 6c), the peaks appear slightly resolved; however, the ToT volumes are significantly reduced due to the energy loss of α-particles while traversing a slightly thicker layer of air.

The representative α-cluster shapes for producing the spectra in figure 6 are presented in figure 7. As can be seen, the central hit intensity (ToT value) varies depending on the incident angle of the α-particles relative to the detector surface. Adjusting the fill factors f_1 and f_2 allowed selection of specific cluster shapes, but was still insufficient to fully resolve the peaks, as demonstrated in supplementary figures; supplementary figure S5 presents α-cluster shapes and the corresponding spectra for $f_1 > 90\%$ and $f_2 > 60\%$, while supplementary figure S6 shows the results for $f_1 > 90\%$ and $f_2 > 80\%$.

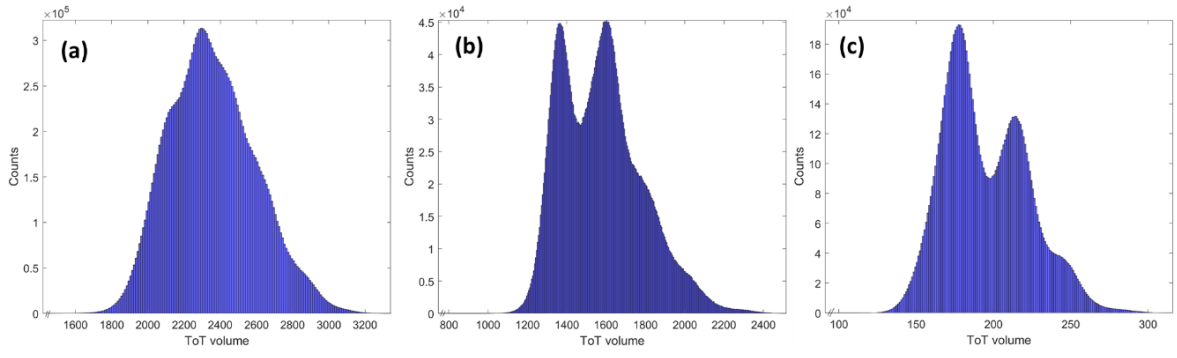

Figure 6. The α-particle energy spectra of the calibration standard (Pu-239, Am-241, and Cm-244), measured with Timepix3 at source-to-detector distances of (a) ~1.1 cm (b) ~2.2 cm (c) ~2.5 cm. These spectra depict the frequency distribution of ToT volumes across all reconstructed α-clusters.

2026 JINST 21 C01010

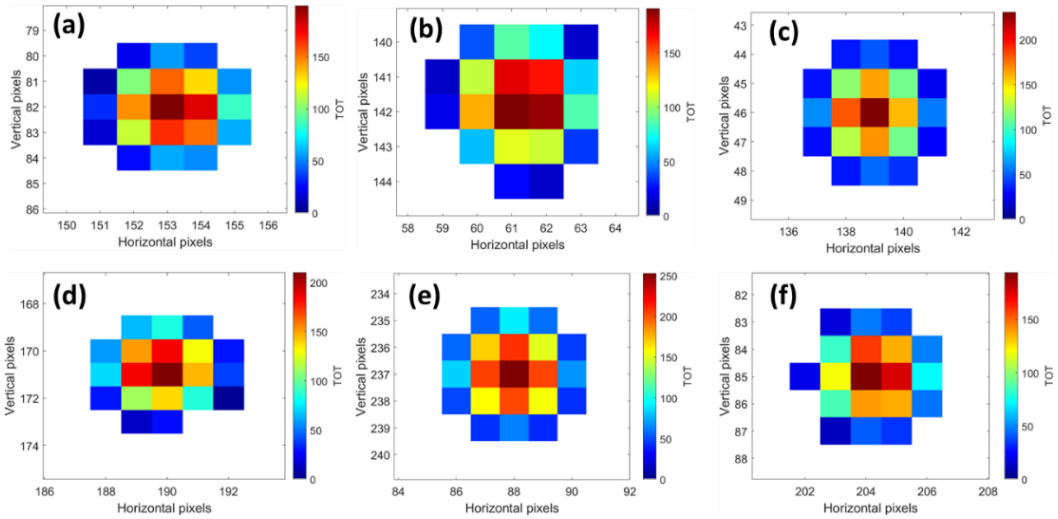

Figure 7. Shapes of various α-particle clusters at different regions of the sensor.

Accepting this as a limitation, we fitted the best spectrum at a 2.2 cm source-to-detector distance. To do this, the histogram shown in figure 6b was first converted into a line spectrum by selecting the center value of each bin as a data point (figure 8a). The resulting line spectrum was then fitted using a sum of four standard Gaussian distribution functions, with the peak ToT volumes fixed at 1368, 1590, 1800, and 2030. This approach produced a satisfactory fit to the data. When the first three ToT volume values were plotted against the corresponding three major α-particle energy peaks at 5.15 MeV (5150 keV), 5.49 MeV (5490 keV), and 5.80 MeV (5800 keV), a linear correlation was obtained (figure 8b).

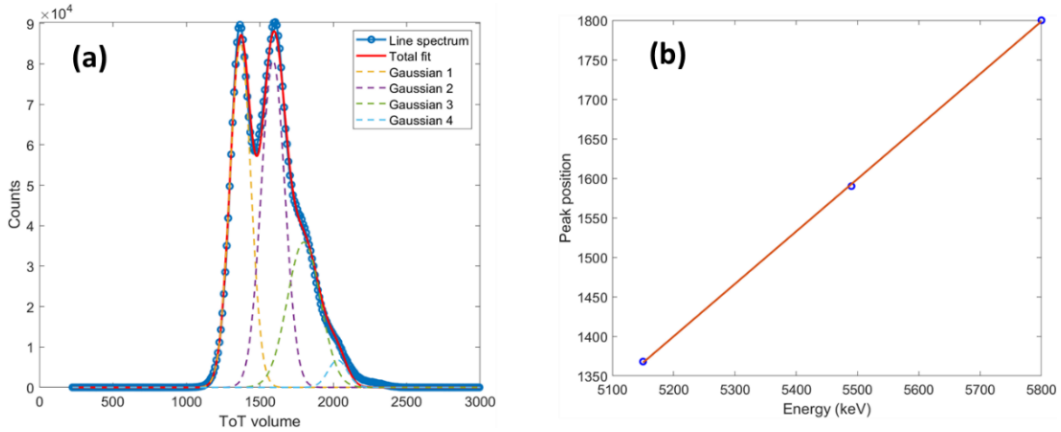

Figure 8. (a) Line spectrum (blue curve) derived from the histogram-based energy spectra presented in figure 6. It was fitted with a sum of four standard Gaussian distribution functions to resolve the overlapping peaks and determine their positions. (b) Linear correlation between the known α-particle peak energies and the peak positions obtained from the fit in (a).

2026 JINST 21 C01010

5 Discussions

In this study, a Timepix3 detector was characterized, and its performance was evaluated for detecting high-energy charged particles (α-particles), aimed at mapping the spatial distribution of K-40, U-238, and Th-232 radionuclides and performing a microdosimetry study for application in luminescence dating. A reconstruction algorithm was developed to reconstruct and identify various particles. One-to-three-pixel hits were identified as photons. Larger clusters (> 5 pixels in size) were further processed to separate β- and α-particles. Using fill factor thresholds $f_1$and f_2 around the central pixel ($f_1 > 90\%$ and $f_2 > 40\%$), α-particle clusters were separated from β-particles with more than 90% accuracy. Varying these thresholds also provided insight into the orientation and energy deposition behavior of α-particles on the sensor. A simple, global (full-chip) calibration approach was adopted to calibrate the detector. The detector was unable to resolve the individual α-particle peaks under the current measurement conditions and detector configuration. The overlap and broadening of peaks are likely due to energy loss in air and to the lack of temperature control and/or vacuum conditions. This is plausible, as previous studies relied on measurements with a single source [11, 12], whereas the mixed α-particle source used here naturally produces more peak overlap and a broader combined spectrum.

A systematic variation of the source-to-detector distance resulted in optimal resolution at ~2.2 cm. Gaussian fitting of the spectrum at this distance separated overlapping peaks, yielding a linear correlation with known α-particles' energies. While α-particle peaks did not fully resolve, calibrating the detector in air provides a more realistic representation of natural sedimentary environments, where α- and β-particles emitted from radionuclides in pore spaces or at grain boundaries also lose energy as they traverse air or partially air-filled microstructures. This approach inherently incorporates the path-length variations, reduced particle energies, and broadened energy spectra.

6 Conclusions

A reconstruction and identification algorithm was developed for separating photons, β-particles (electrons), and α-particles from the mixed radiation fields or maps. While calibrating Timepix3, a source-to-detector distance of ~2.2 cm for our setup provided the best compromise between peak resolution and signal strength. The measured ToT volumes showed a linear correlation with known α-particle energies from the calibration source, validating the detector's energy response under the global calibration approach. Although the Timepix3 detector was unable to fully resolve the individual α-particle peaks under atmospheric conditions, likely due to energy loss in air and lack of temperature stabilization and/or vacuum conditions, calibrating in air remains useful, as the detector is intended for use at ambient atmospheric pressure and within complex mixed radiation fields. Consequently, the calibration, detector characterization, and algorithm development performed in this study form essential preparatory steps toward deploying Timepix3 in low-radioactivity natural settings for mapping energy-resolved α- and β-particle emissions, determining radionuclide distributions at the grain scale, and investigating microdosimetric behavior relevant to luminescence dating.

Acknowledgments

This research was supported by the NERC-funded project NE/ T001313/1.

2026 JINST 21 C01010

Supplementary material and data. The following files are provided as supplementary material/data and are accessible through the article's webpage.

- `Supplementary Figures.pptx` (Preparing Timepix3 for Deployment in Low-Radioactivity Natural Settings: An Integrated Workflow for Charged Particle Detection and Imaging). This file contains six supplementary figures that support the experimental investigations presented in the main text. These figures provide additional information on the experimental setup, data acquisition, and analysis procedures, and offer further insight into the methods and results discussed in the manuscript.

References

[1] D.J. Huntley, D.I. Godfrey-Smith and M.L.W. Thewalt, *Optical dating of sediments*, *Nature* **313** (1985) 105.

[2] M.J. Aitken, *Thermoluminescence Dating*, U.S. ed., Studies in Archaeological Science, Academic Press (1985).

[3] A.S. Murray and R.G. Roberts, *Determining the burial time of single grains of quartz using optically stimulated luminescence*, *Earth Planet. Sci. Lett.* **152** (1997) 163.

[4] R.P. Nathan et al., *Environmental dose rate heterogeneity of beta radiation and its implications for luminescence dating: Monte Carlo modelling and experimental validation*, *Radiat. Meas.* **37** (2003) 305.

[5] N. Chauhan and A. Singhvi, *Distribution in SAR palaeodoses due to spatial heterogeniety of natural beta dose*, *Geochronometria* **38** (2011) 190.

[6] K. Thomas et al., *The μ Dose system: determination of environmental dose rates by combined alpha and beta counting-performance tests and practical experiences*, *Geochronology* **4** (2022) 1.

[7] X. Llopart et al., *Timepix, a 65k programmable pixel readout chip for arrival time, energy and/or photon counting measurements*, *Nucl. Instrum. Meth. A* **581** (2007) 485.

[8] X. Fu et al., *Beta dose heterogeneity in sediment samples measured using a Timepix pixelated detector and its implications for optical dating of individual mineral grains*, *Quat. Geochronol.* **68** (2022) 101254.

[9] E. Frojdh et al., *Timepix3: first measurements and characterization of a hybrid-pixel detector working in event driven mode*, 2015 *JINST* **10** C01039.

[10] J. Jakubek et al., *Selective detection of secondary particles and neutrons produced in ion beam therapy with 3D sensitive voxel detector*, 2011 *JINST* **6** C12010.

[11] M. Sommer, C. Granja, S. Kodaira and O. Ploc, *High-energy per-pixel calibration of timepix pixel detector with laboratory alpha source*, *Nucl. Instrum. Meth. A* **1022** (2022) 165957.

[12] J. Jakubek, *Precise energy calibration of pixel detector working in time-over-threshold mode*, *Nucl. Instrum. Meth. A* **633** (2011) S262.

2026 JINST 21 C01010